

Split of zero-bias conductance peak in normal-metal / d wave superconductor junctions

Yasuhiro Asano*

Department of Applied Physics, Hokkaido University, Sapporo 060-8628, Japan

Yukio Tanaka

Department of Applied Physics, Nagoya University, Nagoya 464-8603, Japan

Satoshi Kashiwaya

National Institute of Advanced Industrial Science and Technology, Tsukuba, 305-8568, Japan

(Dated: October 31, 2018)

Effects of impurity scatterings on the conductance in normal-metal / d wave superconductor junctions are discussed by using the single-site approximation. So far, the split of the zero-bias conductance peak has been believed to be an evidence of the broken time reversal symmetry states at the surface of high- T_c superconductors. In this paper, however, it is shown that the impurity scattering near the interface also causes the split of the zero-bias conductance peak. Typical conductance spectra observed in experiments at finite temperatures and under external magnetic fields are explained well by the present theory.

PACS numbers: 74.81.-g, 74.25.Fy, 74.50.+r

I. INTRODUCTION

The zero-energy state (ZES)¹ formed at surfaces of superconductors is a consequence of the unconventional symmetry of Cooper pairs. Since the ZES appears just on the Fermi energy, it drastically affects transport properties through the interface of junctions consist of unconventional superconductors.² For instance in normal-metal / high- T_c superconductor junctions, a large peak is observed in the differential conductance at the zero bias voltage.^{3,4,5,6,7,8,9,10} The ZES is also responsible for the low-temperature anomaly of the Josephson current between the two unconventional superconductors.^{11,12,13,14,15,16,17,18,19,20,21}

An electron incident into a normal-metal / superconductor (NS) interface suffers the Andreev reflection²² by the pair potential in the superconductor. As a result, a hole traces back the original propagation path of the incident electron. This is called the retro property of a quasiparticle which supports the formation of the ZES. Strictly speaking, the electron-hole pairs just on the Fermi energy hold the retro property in the presence of the time reversal symmetry (TRS). Thus the ZES is sensitive to the TRS of the system. Actually, the zero-bias conductance peak (ZBCP) in NS junctions splits into two peaks under magnetic fields.^{23,24,25,26} The peak splitting is also discussed^{27,28,29,30,31,32,33} when the broken time reversal symmetry state (BTRSS) is formed at the interface. Theoretical studies showed that such BTRSS's are characterized by the $s+id_{xy}$ ²⁸ or $d_{xy}+id_{x^2-y^2}$ ³⁴ wave pairing symmetry. Experimental results, however, are still controversial. Some experiments reported the split of the ZBCP at the zero magnetic field,^{35,36,37,38,39,40,41,42} other did not observe the splitting.^{5,7,8,43,44,45} The ZBCP is also sensitive to the exchange potential in ferromagnets attaching

to unconventional superconductors.^{46,47}

In previous papers, we numerically showed that random potentials at the NS interface cause the split of the ZBCP at the zero magnetic field by using the recursive Green function method.^{48,49} We also showed that the splitting due to the impurity scattering can be seen more clearly when realistic electronic structures of high- T_c materials are taken into account.⁵⁰ Unfortunately, we could not make clear a mechanism of splitting. Our conclusion, however, contradicts to those of a number of theories^{51,52,53,54,55,56} based on the quasiclassical Green function method.^{57,58,59,60,61} The drastic suppression of the ZBCP by the interfacial randomness is the common conclusion of all the theories. The theories of the quasiclassical Green function method, however, concluded that the random potentials do not split the ZBCP. Thus this issue has not been fixed yet. There are mainly two reasons for the disagreement in the two theoretical approaches (i.e., the recursive Green function method and the quasiclassical Green function method). One is the treatment of the random potentials, the other is the effects of the rapidly oscillating wave functions on the conductance. In our simulations, we calculate the conductance without any approximation to the random potentials and the wave functions; this is an advantage of the recursive Green function method.^{49,62}

In this paper, we discuss effects of the impurity scattering on the conductance in normal-metal/ d wave superconductor junctions by using the Lippmann-Schwinger equation. We assume that impurities are near the NS interface on the superconductor side. The differential conductance is analytically calculated within the single-site approximation based on the conductance formula.^{63,64} The split of the ZBCP due to the impurity scattering is the main conclusion of this paper. The impurity scattering affects the conductance in two ways: (i) drastically

suppressing the conductance around the zero bias voltage and (ii) making the conductance peak wider. The split of the ZBCP is a consequence of the interplay between the two effects. In the present theory, we successfully explain typical conductance shapes observed in several experiments. We also show that the splitting peaks are merged into a single conductance peak for sufficiently high temperatures and that the peak splitting width increases with increasing external magnetic fields.

This paper is organized as follows. In Sec. II, we derive the reflection coefficients in NS junctions within the single-site approximation based on the Lippmann-Schwinger equation. The split of the ZBCP is discussed in Sec. III. In Sec. IV, calculated results are compared with experiments and another theories. In Sec. V, we summarize this paper.

II. LIPPMANN-SCHWINGER EQUATION

Let us consider two-dimensional NS junctions as shown in Fig. 1, where normal metals ($x < 0$) and d wave superconductors ($x > 0$) are separated by the potential barrier $V_B(\mathbf{r}) = V_0\delta(x)$. We assume the periodic boundary condition in the y direction and the width of the junction is W . The a axis of high- T_c superconductors is oriented

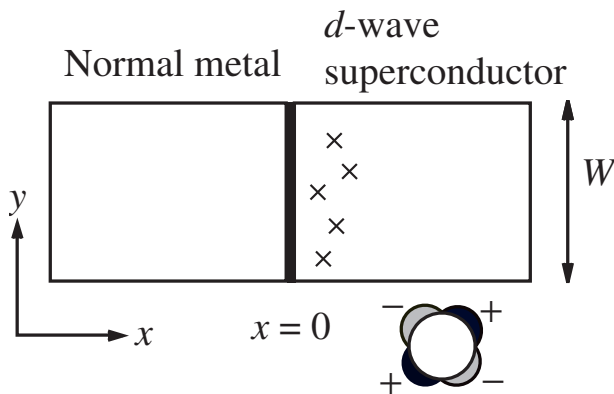


FIG. 1: The normal-metal / d -wave superconductor junction is schematically illustrated. The crosses represent impurities.

by the 45 degrees from the interface normal. The pair potential of a high- T_c superconductor is described by

$$\Delta_{\mathbf{k}} = 2\Delta_0 \bar{k}_x \bar{k}_y, \quad (1)$$

in the momentum space, where Δ_0 is the amplitude of the pair potential at the zero temperature, $\bar{k}_x = \cos \gamma = k_x/k_F$ and $\bar{k}_y = \sin \gamma = k_y/k_F$ are the normalized wave number on the Fermi surface in the x and the y direction, respectively. The Fermi wave number k_F satisfies $\hbar^2 k_F^2 / 2m = \mu_F$, where μ_F is the Fermi energy. The schematic figure of the pair potential is shown in Fig. 1. The NS junctions are described by the Bogoliubov-de

Genes equation,⁶⁵

$$\int d\mathbf{r}' \begin{pmatrix} \delta(\mathbf{r} - \mathbf{r}') h_0(\mathbf{r}') & \Delta(\mathbf{r}, \mathbf{r}') \\ \Delta^*(\mathbf{r}, \mathbf{r}') & -\delta(\mathbf{r} - \mathbf{r}') h_0(\mathbf{r}') \end{pmatrix} \times \begin{pmatrix} u(\mathbf{r}') \\ v(\mathbf{r}') \end{pmatrix} = E \begin{pmatrix} u(\mathbf{r}) \\ v(\mathbf{r}) \end{pmatrix}, \quad (2)$$

$$h_0(\mathbf{r}) = -\frac{\hbar^2 \nabla^2}{2m} + V_{pot}(\mathbf{r}) - \mu_F, \quad (3)$$

$$V_{pot}(\mathbf{r}) = V_B(\mathbf{r}) + V_I(\mathbf{r}), \quad (4)$$

$$\Delta(\mathbf{R}_c, \mathbf{r}_r) = \begin{cases} \frac{1}{V_{vol}} \sum_{\mathbf{k}} \Delta_{\mathbf{k}} e^{i\mathbf{k} \cdot \mathbf{r}_r} & : X_c > 0 \\ 0 & : X_c < 0 \end{cases}, \quad (5)$$

where $\mathbf{R}_c = (X_c, Y_c) = (\mathbf{r} + \mathbf{r}')/2$ and $\mathbf{r}_r = \mathbf{r} - \mathbf{r}'$. Throughout this paper, we neglect the spatial dependence of the pair potential near the junction interface. This is a reasonable approximation when we consider the conductance around the zero bias voltage.⁶⁶ The spatial dependence of the pair potential should be determined in a self-consistent way when we discussed the conductance far from the zero bias such as $eV \sim \Delta_0$. Here V is the bias voltage applied to junctions.

We consider impurities near the interface on the superconductor side as indicated by crosses in Fig. 1. The potential of impurities is given by

$$V_I(\mathbf{r}) = V_i \sum_{j=1}^{N_i} \delta(\mathbf{r} - \mathbf{r}_j), \quad (6)$$

where N_i is the number of impurities. In the absence of impurities, the transmission and the reflection coefficients are calculated from boundary conditions of wave functions at the junction interface as shown in Appendix A. By using these coefficients, four retarded Green functions are obtained as shown in Appendix B. The normal conductance of the junction is given by

$$G_N = \frac{2e^2}{h} N_c T_B, \quad (7)$$

$$T_B = \int_0^{\pi/2} d\gamma \frac{\cos^3 \gamma}{z_0^2 + \cos^2 \gamma}, \quad (8)$$

where T_B is the transmission probability of the junction, $N_c = 2W/\lambda_F$ is the number of the propagating channels on the Fermi surface, $\lambda_F = 2\pi/k_F$ is the Fermi wave length and $z_0 = mV_0/(\hbar^2 k_F)$ represents the strength of the potential barrier at the NS interface. In the limit of $z_0^2 \gg 1$, T_B is proportional to $1/z_0^2$.

Effects of impurities on the wave functions are taken into account by using the Lippmann-Schwinger equation,

$$\psi^{(l)}(\mathbf{r}) = \psi_0^{(l)}(\mathbf{r}) + \int d\mathbf{r}' \hat{G}_0(\mathbf{r}, \mathbf{r}') V_I(\mathbf{r}') \hat{\sigma}_3 \psi^{(l)}(\mathbf{r}'), \quad (9)$$

$$= \psi_0^{(l)}(\mathbf{r}) + \sum_{j=1}^{N_i} \hat{G}_0(\mathbf{r}, \mathbf{r}_j) V_i \hat{\sigma}_3 \psi^{(l)}(\mathbf{r}_j), \quad (10)$$

where l indicates a propagating channel characterized by the transverse wave number $k_y^{(l)}$. Here $\psi_0^{(l)}(\mathbf{r})$ is the wave function in which an electronlike quasiparticle with $k_y^{(l)}$ is incident into the clean NS interface from normal metals and is described as

$$\psi_0^{(l)}(\mathbf{r}) = \chi_l(y) \left[\begin{pmatrix} 1 \\ 0 \end{pmatrix} e^{iq_l^+ x} + \begin{pmatrix} 0 \\ 1 \end{pmatrix} e^{iq_l^- x} r_{NN}^{he}(l) + \begin{pmatrix} 1 \\ 0 \end{pmatrix} e^{-iq_l^+ x} r_{NN}^{ee}(l) \right], \quad (11)$$

$$\chi_l(y) = \frac{e^{ik_y^{(l)}y}}{\sqrt{W}}, \quad (12)$$

for $x < 0$, where $q_l^\pm = \sqrt{k_l^2 \pm k_F^2 E/\mu_F}$ is the wave number of a quasiparticle in normal metals and $k_l^2 + k_y^{(l)2} = k_F^2$. For $x > 0$, the wave function in clean junctions is given by

$$\psi_0^{(l)}(\mathbf{r}) = \chi_l(y) \hat{\Phi} \left[\begin{pmatrix} u_l \\ v_l \end{pmatrix} e^{ik_l^+ x} t_{SN}^{ee}(l) + \begin{pmatrix} -v_l \\ u_l \end{pmatrix} e^{-ik_l^- x} t_{SN}^{he}(l) \right], \quad (13)$$

$$u_l = \sqrt{\frac{E + \Omega_l}{2E}}, \quad (14)$$

$$v_l = \text{sgn}(k_y^{(l)}) \sqrt{\frac{E - \Omega_l}{2E}}, \quad (15)$$

$$\hat{\Phi} = \begin{pmatrix} e^{i\varphi} & 0 \\ 0 & e^{-i\varphi} \end{pmatrix}, \quad (16)$$

where φ is a macroscopic phase of a superconductor, $k_l^\pm = (k_l^2 \pm k_F^2 \Omega_l/\mu_F)^{1/2}$ is the wave number of a quasiparticle in superconductors, $\Omega_l = \sqrt{E^2 - \Delta_l^2}$ and $\Delta_l = 2\Delta_0 \bar{k}_l \bar{k}_y^{(l)}$. The wave function at an impurity $\psi^{(l)}(\mathbf{r}_{j'})$ can be obtained by $\mathbf{r} \rightarrow \mathbf{r}_{j'}$ in Eq. (10)

$$\psi_0^{(l)}(\mathbf{r}_{j'}) = \sum_{j=1}^{N_i} \left[\hat{\sigma}_0 \delta_{j,j'} - \hat{G}_0^{SS}(\mathbf{r}_{j'}, \mathbf{r}_j) V_i \hat{\sigma}_3 \right] \psi^{(l)}(\mathbf{r}_j). \quad (17)$$

It is possible to calculate the exact conductance if we obtain $\psi^{(l)}(\mathbf{r}_j)$ for all impurities by solving Eq. (17). Actually it was confirmed that the conductance calculated from the numerical solution of Eq. (17) is exactly identical to that computed in another numerical methods such as the recursive Green function method.^{62,67} In this paper, we solve Eq. (17) within the single-site approximation, where the multiple scattering effect involving many impurities (Anderson localization) are neglected. However the multiple scattering by an impurity is taken into account up to the infinite order of the scattering events.

In the summation of j in Eq. (17), only the contribution with $j = j'$ is taken into account in the single-site approximation.⁶⁸ In this way, the wave function at \mathbf{r}_j is approximately given by

$$\psi^{(l)}(\mathbf{r}_j) \approx \left[\hat{\sigma}_0 - \hat{G}_0^{SS}(\mathbf{r}_j, \mathbf{r}_j) V_i \hat{\sigma}_3 \right]^{-1} \psi_0^{(l)}(\mathbf{r}_j). \quad (18)$$

We note that the single-site approximation yields the exact conductance when $N_i = 1$. Within the single-site approximation, Eq. (10) can be solved as

$$\psi_{\text{SSA}}^{(l)}(\mathbf{r}) = \psi_0^{(l)}(\mathbf{r}) + \sum_j^{N_i} \hat{G}_0^{NS}(\mathbf{r}, \mathbf{r}_j) V_i \hat{\sigma}_3 \times \left[\hat{\sigma}_0 - \hat{G}_0^{SS}(\mathbf{r}_j, \mathbf{r}_j) V_i \hat{\sigma}_3 \right]^{-1} \psi_0^{(l)}(\mathbf{r}_j), \quad (19)$$

for $x < 0$. On the right hand side of Eq. (19), all functions have been given by analytical expressions.

In the presence of the impurity scattering, the wave function Eq. (19) can be expressed as

$$\psi_{\text{SSA}}^{(l)}(\mathbf{r}) = \begin{pmatrix} 1 \\ 0 \end{pmatrix} \chi_l(y) e^{iq_l^+ x} + \sum_{l'} \chi_{l'}(y) \left[\begin{pmatrix} 0 \\ 1 \end{pmatrix} e^{iq_{l'}^- x} A_{l',l} + \begin{pmatrix} 1 \\ 0 \end{pmatrix} e^{-iq_{l'}^+ x} B_{l',l} \right], \quad (20)$$

for $x < 0$, where $A_{l',l}$ and $B_{l',l}$ are the Andreev and the normal reflection coefficients in the presence of impurities, respectively. These coefficients are obtained from relations

$$\int_{-W/2}^{W/2} dy \chi_m^*(y) (0, 1) \psi_{\text{SSA}}^{(l)}(\mathbf{r}) = e^{iq_m^- x} A_{m,l}, \quad (21)$$

$$\int_{-W/2}^{W/2} dy \chi_m^*(y) (1, 0) \psi_{\text{SSA}}^{(l)}(\mathbf{r}) = e^{iq_l^+ x} \delta_{l,m} + e^{-iq_m^+ x} B_{m,l}. \quad (22)$$

The scattering theory based on the Lippmann-Schwinger equation requires complicated algebra as shown below because the perturbation expansion is carried out in the real space. In return, effects of the impurity scattering can be taken into account up to the infinite order of the perturbation expansion without using any self-consistent treatments. In addition, the reflection coefficients are explicit functions of the impurity positions in a single disordered sample. These are advantages of the present method.

In what follows, we consider low transparent junctions, (i.e., $z_0^2 \gg 1$). From the reflection coefficients in Appendix A, the Green function in the superconductor is given by

$$\begin{aligned} \hat{G}_0^{SS}(\mathbf{r}, \mathbf{r}) = & -i\pi N_0 \frac{2}{\pi} \int_0^{\pi/2} d\gamma \left[\frac{E}{2\Omega} \hat{\sigma}_0 - \frac{z_0^2 \Delta_0^2 e^{2ipx}}{2\Xi\Omega} \hat{\sigma}_0 + \frac{z_0^2 \Delta_0^2 \cos(2k_F x \cos \gamma) e^{2ipx}}{2\Xi\Omega} \hat{\sigma}_0 \right. \\ & - \frac{z_0^2 E}{2\Xi} \left\{ \frac{E}{\Omega} \cos(2k_F x \cos \gamma) \hat{\sigma}_0 + i \sin(2k_F x \cos \gamma) \hat{\sigma}_3 \right\} e^{2ipx} - \frac{\Delta_0^2 \cos^2 \gamma e^{2ipx}}{4\Omega\Xi} \hat{\sigma}_0 \\ & \left. - \frac{z_0 \cos \gamma}{2\Xi} e^{2ipx} \{ E \cos(2k_F x \cos \gamma) \hat{\sigma}_3 + i\Omega \sin(2k_F x \cos \gamma) \hat{\sigma}_0 \} \right], \end{aligned} \quad (23)$$

where $p \approx \frac{k_F}{2 \cos \gamma} \frac{\Omega}{\mu_F}$. The local density of states⁶⁹ at \mathbf{r} is defined by

$$N_s(E, x) = -\frac{1}{\pi} \text{Im Tr } \hat{G}_0^{SS}(\mathbf{r}, \mathbf{r}). \quad (24)$$

The first term in Eq. (23) contributes to the bulk density of states. Since $2p$ is roughly estimated to be i/ξ_0 , another terms contribute to the local density of states near the interface, where $\xi_0 = \hbar v_F / \pi \Delta_0$ is the coherence length and $v_F = \hbar k_F / m$ is the Fermi velocity. In low transparent junctions, 6th, 7th and 8th terms are negligible. The 4th and the 5th terms are also negligible because integrals of such rapidly oscillating functions become very small. The 2nd and 3rd terms are dominant for $E \ll \Delta_0$. In Fig. 2 (a), we show the trace of the Green function in Eq. (23) as a function of E , where $z_0=10$, $\Delta_0 = 0.1\mu_F$, $xk_F = 6$, and $N_0 = m/(\pi\hbar^2)$ is the normal density of states in the unit area. Since $\xi_0 k_F \sim 6.3$, the results correspond to the Green function at a distance ξ_0 away from the interface. The horizontal axis in Fig. 2 (a) is normalized by

$$E_{ZEP} \equiv \frac{\Delta_0}{z_0^2}. \quad (25)$$

The solid and the broken lines represent negative of the imaginary part and the real part of Eq. (23), respectively. As shown in Fig. 2 (a), the imaginary part of the Green function has a large peak around $E = 0$ reflecting the ZES formed at the junction interface. The energy scale, E_{ZEP} , characterizes the width of the zero-energy peak. The real part of the Green function first increases with decreasing E then suddenly decreases to zero for $E \rightarrow 0$. The detail analysis indicates that the real part of the Green function has its maximum around an energy

$$E_{\text{dip}} \equiv \frac{\Delta_0}{z_0^2 (xk_F)^3}. \quad (26)$$

The Green function for $E < E_{ZEP}$ is approximately calculated from the 2nd and the 3rd terms of Eq. (23)

$$\hat{G}_0^{SS}(\mathbf{r}, \mathbf{r}) \approx 2\pi N_0 z_0^2 e^{-x/\xi_0} (g_2 - ig_1) \hat{\sigma}_0, \quad (27)$$

$$g_1 = \frac{2}{\pi} \int_0^{\pi/2} d\gamma \frac{\Delta_0^2 \cos^4 \gamma \sin^2 \gamma \sin^2(xk_F \cos \gamma)}{E^2 z_0^4 + \Delta_0^2 \cos^6 \gamma \sin^2 \gamma}, \quad (28)$$

$$g_2 = \frac{2}{\pi} \int_0^{\pi/2} d\gamma \frac{E z_0^2 \Delta_0 \cos \gamma \sin \gamma \sin^2(xk_F \cos \gamma)}{E^2 z_0^4 + \Delta_0^2 \cos^6 \gamma \sin^2 \gamma}, \quad (29)$$

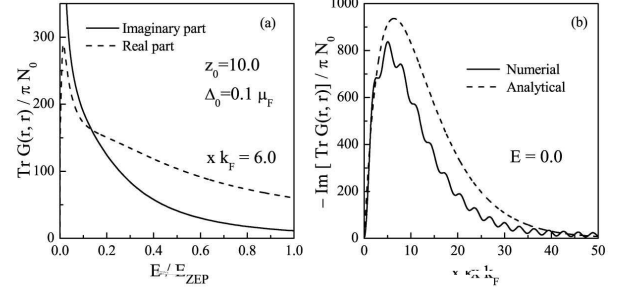


FIG. 2: In (a), the trace of the Green function in the superconductor is shown as a function of E , where $z_0 = 10$, $xk_F = 6$ and $\Delta_0 = 0.1\mu_F$. The peak width of the imaginary part is given by $E_{ZEP} = \Delta_0/z_0^2$. The energy scale, E_{dip} , characterizes the drastic increase of the imaginary part and the drastic decrease of the real part. In (b), the local density of states is shown as a function of xk_F , where $E = 0$, $z_0 = 10$ and $\Delta_0 = 0.1\mu_F$. The numerical and the analytical results are denoted by the solid and the broken lines, respectively.

where we use $\Omega \sim i|2\Delta_0 \cos \gamma \sin \gamma|$. The imaginary part of the Green function, g_1 , is of the order of unity when $E \sim E_{ZEP}$. However, g_1 at $E = 0$ becomes much larger than unity for $xk_F \gg 1$ because

$$g_1(E = 0) = \frac{2}{\pi} \int_0^{\pi/2} d\gamma \frac{\sin^2 \{xk_F \cos \gamma\}}{\cos^2 \gamma} \sim xk_F. \quad (30)$$

Thus the energy scale, E_{dip} , characterizes the drastic increase of g_1 and the drastic decrease of g_2 . The local density of states at $E = 0$ calculated from Eqs. (23) and (24) is plotted as a function of xk_F in Fig. 2(b) with the solid line. For comparison, we also show the analytical results represented by

$$-\text{Im } \hat{G}_0^{SS}(\mathbf{r}, \mathbf{r}) \Big|_{E=0} \simeq 2\pi N_0 z_0^2 e^{-x/\xi_0} xk_F \hat{\sigma}_0, \quad (31)$$

with the broken line. The results show the remarkable enhancement of the local density of states around $x \sim \xi_0$. This implies that the ZES is formed around $x \sim \xi_0$.

Here we note several remarks as follows. To calculate the Green function, we consider the 3rd term in Eq.(23) which rapidly oscillates as $\cos(2xk_F \cos \gamma)$. Such rapidly

oscillating terms are usually neglected in the quasiclassical Green function method. We, however, cannot neglect the 3rd term because it removes the divergence of the local density of state at $E = 0$.^{70,71} The 3rd term also becomes important when we calculate the local density of states just at the surface, (i.e., $x = 0$),

$$\frac{N_s(E, 0)}{N_0} = \text{Re} \frac{2}{\pi} \int_0^{\pi/2} d\gamma \left[\frac{E}{\Omega} - \frac{2E^2 z_0^2 + \Delta_{\mathbf{k}}^2 \cos^2 \gamma}{2\xi\Omega} \right], \quad (32)$$

$$\simeq \frac{2}{\pi} K\left(\frac{\Delta_0}{E}\right) + \frac{2}{\pi} \int_0^{\pi/2} d\gamma \frac{E^2 z_0^2 + \Delta_0^2 \cos^6 \gamma \sin^2 \gamma}{E^2 z_0^4 + \Delta_0^2 \cos^6 \gamma \sin^2 \gamma}, \quad (33)$$

where $K(x)$ is the complete elliptic integral of the first kind and describes the bulk density of states. Another terms come from the 4th and 6th terms in Eq. (23). The first equation is the exact expression and we use $E < E_{\text{ZEP}}$ in the second line. We exactly obtain $N(E = 0, x = 0) = N_0$. Thus there is no remarkable enhancement in the zero energy local density of states just at the interface. The 2nd and the 3rd terms in Eq. (23) do not contribute to the $N_s(E, 0)$ because they exactly cancel with each other at $x = 0$.

In the next section, the conductance for $E < E_{\text{ZEP}}$ will be discussed. It is possible to rewrite a part of Eq. (19) as

$$\left[\hat{\sigma}_0 - V_i \hat{G}_0^{SS}(\mathbf{r}, \mathbf{r}) \hat{\sigma}_3 \right]^{-1} = \frac{\hat{\sigma}_0 + s \hat{\sigma}_3}{1 - s^2}, \quad (34)$$

$$s_1 = Q_0 g_1, \quad (35)$$

$$s_2 = Q_0 g_2, \quad (36)$$

$$Q_0 = 2\pi V_i N_0 z_0^2 e^{-x/\xi_0}, \quad (37)$$

$$s = s_2 - i s_1, \quad (38)$$

where s corresponds to the self-energy of a quasiparticle scattered by an impurity once and describes two important features. First, s becomes large in low transparent junctions even if $V_i N_0$ is fixed at a small constant because Q_0 in Eq.(37) is proportional to $V_i N_0 z_0^2 \sim V_i N_0 / T_B$. Thus Q_0 represents the normalized strength of the impurity scattering. This behavior explains the previous numerical simulation.⁴⁸ Second, effects of impurity scattering far away from the interface on the conductance is negligible because Q_0 decreases exponentially with the increase of x . Impurities around the ZES, (i.e., $x \sim \xi_0$) seriously affect the conductance for $E < E_{\text{ZEP}}$.

III. CONDUCTANCE

The differential conductance in NS junctions is calculated from the normal and the Andreev reflection coeffi-

cients,^{63,64}

$$G_{NS}(eV) = \frac{2e^2}{h} \sum_{l,m} \int_{-\infty}^{\infty} dE \left(\frac{\partial f_{\text{FD}}(E - eV)}{\partial(eV)} \right) \times [\delta_{l,m} - |\bar{B}_{m,l}(E)|^2 + |\bar{A}_{m,l}(E)|^2], \quad (39)$$

$$\bar{A}_{m,l} = \sqrt{\frac{k_m}{k_l}} A_{m,l}, \quad (40)$$

$$\bar{B}_{m,l} = \sqrt{\frac{k_m}{k_l}} B_{m,l}, \quad (41)$$

where $f_{\text{FD}}(E)$ is the Fermi-Dirac distribution function. When $z_0^2 \gg 1$ and $E < E_{\text{ZEP}}$, the reflection coefficients are calculated as

$$\bar{A}_{m,l} = \delta_{l,m} r_{NN}^{he}(l) + e^{-i\varphi} L_{m,l} [\Delta_m |\Delta_l|(s+1) + \Delta_l |\Delta_m|(s-1)], \quad (42)$$

$$\bar{B}_{m,l} = \delta_{l,m} r_{NN}^{ee}(l) + i L_{m,l} [|\Delta_m| |\Delta_l|(s+1) + \Delta_l \Delta_m (s-1)], \quad (43)$$

$$L_{m,l} = \frac{\pi N_0 V_i z_0^2}{(1-s^2) k_F} \sum_{j=1}^{N_i} \chi_l(y_j) \chi_m^*(y_j) \times \frac{\sqrt{k_l k_m}}{\Xi_l \Xi_m} e^{i(p_m + p_l)x_j} \sin(k_m x_j) \sin(k_l x_j). \quad (44)$$

The conductance is then given by

$$G_{NS} = \frac{2e^2}{h} \int_{-\infty}^{\infty} dE \left(\frac{\partial f_{\text{FD}}(E - eV)}{\partial(eV)} \right) \times \left[N_c g^{(0)} - 4 \sum_{j=1}^{N_i} \Gamma_j \right], \quad (45)$$

$$g^{(0)} = 2 \int_0^{\pi/2} d\gamma \frac{\Delta_0^2 \cos^7 \gamma \sin^2 \gamma}{E^2 z_0^4 + \Delta_0^2 \cos^6 \gamma \sin^2 \gamma}, \quad (46)$$

$$\Gamma_j = \text{Re} \frac{s Q_0 (2I_2 - iI_1 + iI_3)}{s^2 - 1}, \quad (47)$$

$$I_1 = \frac{2}{\pi} \int_0^{\pi/2} d\gamma \frac{\Delta_0^4 \cos^{10} \gamma \sin^4 \gamma \sin^2(x_j k_F \cos \gamma)}{(E^2 z_0^4 + \Delta_0^2 \cos^6 \gamma \sin^2 \gamma)^2}, \quad (48)$$

$$I_2 = \frac{2}{\pi} \int_0^{\pi/2} d\gamma \frac{E z_0^2 \Delta_0^3 \cos^7 \gamma \sin^3 \gamma \sin^2(x_j k_F \cos \gamma)}{(E^2 z_0^4 + \Delta_0^2 \cos^6 \gamma \sin^2 \gamma)^2}, \quad (49)$$

$$I_3 = \frac{2}{\pi} \int_0^{\pi/2} d\gamma \frac{E^2 z_0^4 \Delta_0^2 \cos^4 \gamma \sin^2 \gamma \sin^2(x_j k_F \cos \gamma)}{(E^2 z_0^4 + \Delta_0^2 \cos^6 \gamma \sin^2 \gamma)^2}. \quad (50)$$

The first term of Eq. (45), $N_c g^{(0)}$, is the conductance in clean junctions and Γ_j represents effects of the impurity scattering on the conductance. When we calculate $|\bar{A}_{m,l}|^2$ and $|\bar{B}_{m,l}|^2$, the summation with respect to impurities $\sum_j^{N_i} \sum_{j'}^{N_i}$ must be carried out only for $j' = j$ in the single-site approximation.⁶⁸ As a consequence, the current conservation law is satisfied for $E < E_{\text{ZEP}}$.

To study effects of impurities on the conductance, we first assume $x_j = x_0$ for all impurities. The conductance

is rewritten as

$$G_{NS} = \frac{2e^2}{h} \int_{-\infty}^{\infty} dE \left(\frac{\partial f_{\text{FD}}(E - eV)}{\partial(eV)} \right) \times N_c \left[g^{(0)} - 2n_i \Gamma_j \right], \quad (51)$$

where $n_i = N_i \lambda_F / W$ is the dimensionless line density of impurities less than unity. When scattering effects are strong, $|s| \gg 1$, N_i cannot be much larger than W / λ_F . This limits the applicability of the single-site approximation.

We show conductance for several choices of $x_0 k_F$ and $V_i N_0$ in Fig. 3, where $z_0 = 10$ and $n_i = 0.9$. The two parameters are chosen as $x_0 k_F = 10$, $V_i N_0 = 0.01$ in (a), $x_0 k_F = 2.0$, $V_i N_0 = 0.005$ in (b), $x_0 k_F = 26.0$, $V_i N_0 = 0.1$ in (c) and $x_0 k_F = 12.0$, $V_i N_0 = 0.1$ in (d). The broken line is the conductance in clean junctions. The temperature is fixed at a very low temperature $T = 0.01 E_{\text{ZEP}}$ which is estimated to be 0.05 K by using $\Delta_0 = 50$ meV for $z_0 = 10$. As shown in (a)-(c), the ZBCP is splitting into two peaks by the impurity scattering. While the results in (d) shows the single ZBCP. Roughly

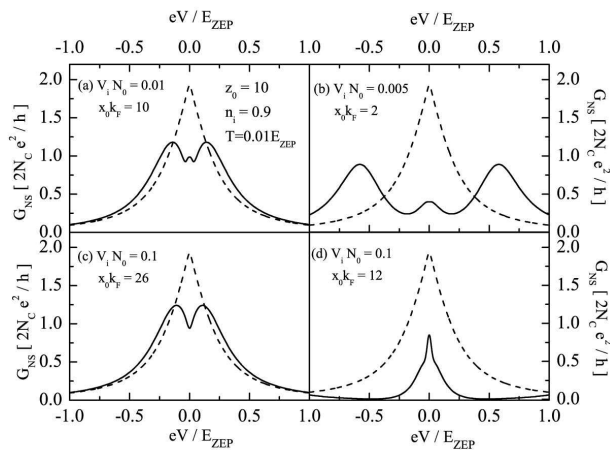


FIG. 3: The conductance is plotted as a function of bias voltages, where $z_0 = 10$ and $n_i = 0.9$. The parameters are $x_0 k_F = 10$, $V_i N_0 = 0.01$ in (a), $x_0 k_F = 2.0$, $V_i N_0 = 0.005$ in (b), $x_0 k_F = 26$, $V_i N_0 = 0.1$ in (c) and $x_0 k_F = 12$, $V_i N_0 = 0.1$ in (d). The broken lines denote the conductance in clean junctions.

speaking, the impurity scattering affects the ZBCP in two ways: (i) it decreases the conductance around the zero bias voltage and (ii) it makes the ZBCP wider. The two effects (i) and (ii) are well characterized by the E dependence of Γ_j and the sign change of Γ_j in Eq. (51), respectively. In Fig. 4, Γ_j is plotted as a function of E for several $x_0 k_F$, where $V_i N_0$ is fixed at 0.01. We note that Γ_j for $x_0 k_F = 10$ yields the conductance in Fig. 3 (a). When $x_0 k_F \gg \xi_0$, $\Gamma_j \sim 0$ and impurity

scattering is negligible as shown for $x_0 k_F = 50$ because Q_0 in Eq. (37) becomes almost zero. For $x_0 k_F = 2, 5$ and 10 , Γ_j increases with decreasing E , which indicates the enhancement of the impurity scattering around $E = 0$. The suppression of the conductance around the zero bias is explained in terms of the drastic increase of the local density of states with decreasing E as shown in Fig. 2 (a). Therefore the suppression of the zero-bias conductance happens irrespective of $x_0 k_F$ and $V_i N_0$. In addition, a nonmonotonic E dependence of Γ_j for $x_0 k_F = 10$ is a source of small conductance peak at the zero-bias in Fig. 3 (a). The same small peak is also found in Fig. 3 (b).

The widening of the ZBCP can be explained by the sign change of Γ_j . When $E > 0.15 E_{\text{ZEP}}$ in Fig. 4, Γ_j for $x_0 k_F = 10$ becomes negative and impurities enhance the conductance. As a consequence, the conductance peak becomes wider than $g^{(0)}$. The split of the ZBCP is a consequence of the interplay between the suppression of the conductance around the zero bias voltage and the widening of the ZBCP as shown in Fig. 3 (a)-(c). Therefore the sign change of Γ_j explains the split of the ZBCP. For $E_{\text{dip}} < E < E_{\text{ZEP}}$, Γ_j is almost a decreasing function

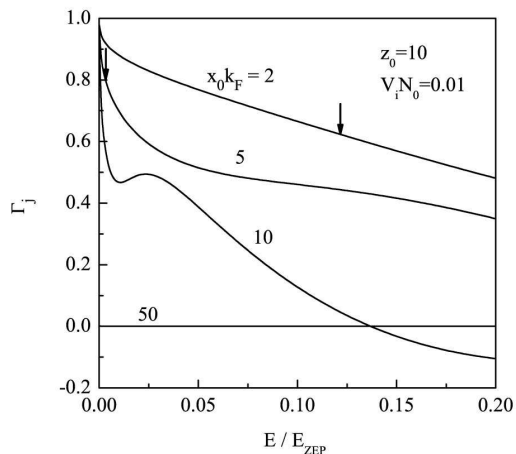


FIG. 4: The function $\Gamma_j(E)$ is plotted as a function of E for several $x_0 k_F$ at $V_i N_0 = 0.01$. The arrows indicate E_{dip} . For $x_0 k_F = 10$, $E_{\text{dip}} = 0.001 E_{\text{ZEP}}$.

of E and is positive at $E = E_{\text{dip}}$ as shown in Fig. 4. It is followed from Eq. (47) that

$$\Gamma_j \propto |s|^2 \{s_1(I_1 - I_3) + 2I_2 s_2\} + \{s_1(I_1 - I_3) - 2I_2 s_2\}. \quad (52)$$

Within our study, $s_1(I_1 - I_3)$ tends to be much smaller than $2I_2 s_2$ for $E_{\text{dip}} < E < E_{\text{ZEP}}$, which implies an importance of the real part of the self-energy, s_2 , for the splitting. The sign change of Γ_j happens when the impurity scattering is sufficiently weak so that

$$|s|^2 = s_1^2 + s_2^2 \sim 1, \quad (53)$$

is satisfied. When $|s(E = E_{\text{dip}})|$ is a small value less than unity, the effects of impurities are negligible and the conductance almost remains unchanged from that in clean junctions. The split also cannot be seen when $|s(E = E_{\text{ZEP}})|$ is larger than unity. An example is shown in Fig. 3(d), where $x_0 k_F = 12.0$, $V_i N_0 = 0.1$ and $|s(E = E_{\text{ZEP}})|$ is estimated to be 1.5. In this case, the suppression of the zero-bias conductance dominates over the widening of the ZBCP. As a result, the conductance is always smaller than that in clean junctions and the ZBCP remains in a single peak.

We should pay attention to a similarity in the shapes of the conductance in the present theory and those in experiments. Amazingly, the conductance structure in Fig. 3 (a) is very similar to that observed in the experiment³⁵. It is possible to find a very small conductance peak at $V = 0$ in addition to the splitting peaks around $V \sim \pm 1\text{mV}$ in Fig. 2 of Ref. 35. The impurities away from the interface explains another conductance shape in the experiment⁸. The conductance structure in Fig. 2 of Ref. 8 is very similar to that in Fig. 3 (d). The present theory explains, at least, two typical conductance shapes observed in the experiments.

As shown in Fig. 3, the magnitude of the impurity potential and the position of impurities are key factors for the degree of splitting. In Fig. 5, the gray area indicates sets of $(V_i N_0, x_0 k_F)$ which satisfy Eq. (53) within $E_{\text{dip}} < E < E_{\text{ZEP}}$. The open circles denote sets of $(V_i N_0, x_0 k_F)$, where we find the split of the ZBCP in Eq. (51). All the circles are inside of the gray area.

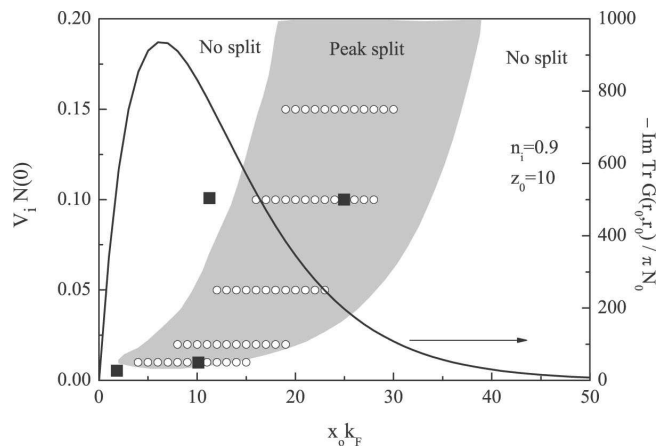


FIG. 5: A phase diagram for the split of the ZBCP. The gray area indicates sets of $(V_i N_0, x_0 k_F)$ which satisfy Eq. (53). The open circles denote sets of $(V_i N_0, x_0 k_F)$, where we find the split of the ZBCP in Eq. (51). The local density of state at $E = 0$ in Fig. 2 (b) is also shown. The filled squares are parameters used for the conductance in Fig. 3.

Although the circles and the gray region are not perfectly coincide with each other, they show qualitatively the same tendency. The parameters used in Fig. 3 are indicated by filled squares. Since s at $E = 0$ is proportional to the local density of states, we also show the

$N_s(E = 0, x)$ in Eq. (31). To satisfy Eq. (53), impurities around $x_0 \sim \xi_0$ should have sufficiently small scattering potentials because the local density of states has large values there. Thus the gray area appears for small impurity potentials near the interface, (i.e., $x_0 \lesssim \xi_0$). The gray region spreads to larger $V_i N_0$ as the increase of $x_0 > \xi_0$ because the local density of states becomes smaller values. The results imply that the strong impurities are not necessary for the split of the ZBCP. It is evident that this phase diagram is valid in the limit of high impurity density and the diagram would be changed depending on the transmission probability of junctions.

In Fig. 3, all impurities are aligned at $x_j = x_0$. In real junctions, however, impurities may be distributed randomly near the interface as shown in Fig. 1. The conductance in such realistic junctions are shown in Fig. 6, where impurities are distributed randomly in the range of $1 < x_j k_F < L_s k_F$, $\rho_i = N_i \frac{\lambda_F^2}{W L_s}$ is the dimensionless area density of impurities and $z_0 = 10$. The conductance is calculated from an expression

$$G_{NS} = \frac{2e^2}{h} N_c \int_{-\infty}^{\infty} dE \left(\frac{\partial f_{\text{FD}}(E - eV)}{\partial(eV)} \right) \times \left[g^{(0)} - \rho_i \frac{k_F L_s}{\pi} \langle \Gamma \rangle \right], \quad (54)$$

$$\langle \Gamma \rangle = \left\langle \frac{1}{N_i} \sum_{j=1}^{N_i} \Gamma_j \right\rangle, \quad (55)$$

where $\langle \dots \rangle$ represents the ensemble average. Since the conductance in Eq. (45) is characterized by the number of impurities, a factor $k_F L_s / \pi$ appears in Eq. (54). We choose $L_s k_F = 20$ in Fig. 6 because we focus on the impurities near the interface and $\xi_0 k_F \sim 6.3$. We consider low density strong impurities in (a), where $V_i N_0 = 0.1$ and $\rho_i = 0.2$. There is no peak splitting in Fig. 6 (a) because most impurities are outside of the gray region in Fig. 5. On the other hand, the results in Fig. 6 (b) show the split of the ZBCP at $T = 0$, where we consider high density weak impurities with for $V_i N_0 = 0.02$ and $\rho_i = 0.6$. This is because most impurities are inside of the gray region in Fig. 5. The splitting peaks merge into a single peak under finite temperatures such as $T = 0.1 E_{\text{ZEP}}$. In Fig. 6 (c), we show the temperature dependence of the zero-bias conductance in Fig. 6 (b). The results show the reentrant behavior of the zero-bias conductance, which was found in the experiment.³⁵ In Fig. 6 (d), the peak position (δeV) in (b) is plotted as a function temperatures. Since δeV is about $0.15 E_{\text{ZEP}}$ at $T = 0$, peak splitting is washed out at high temperatures such as $T = 0.11 E_{\text{ZEP}}$. High density impurities with weak random potential are responsible for the split of the ZBCP in low transparent junctions.

Several experiments^{35,40} show a sensitivity of the conductance peaks to external magnetic fields. Here we discuss the conductance in the presence of magnetic fields. The effects of magnetic fields are taken into account phenomenologically by using the Aharonov-Bohm like phase

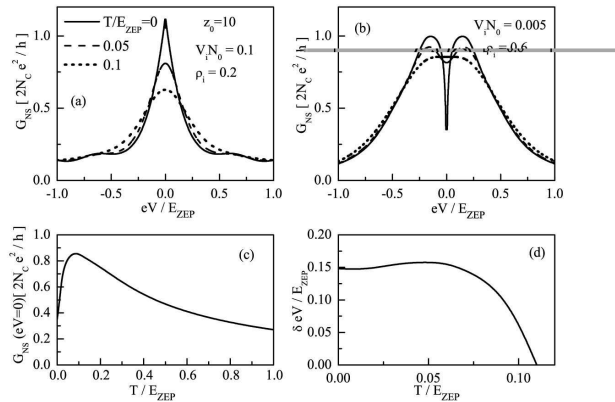


FIG. 6: The conductance in the presence of impurities distributed randomly in the range of $1 < x_j k_F < 20$, where ρ_i is the dimensionless area density of impurities near the interface. The conductance for low density strong impurities is shown in (a) with $V_i N_0 = 0.1$ and $\rho_i = 0.2$. The conductance for high density weak impurities with $V_i N_0 = 0.005$ and $\rho_i = 0.6$ are shown for several choices of temperatures. The zero-bias conductance and the peak positions in (b) are plotted as a function of temperatures in (c) and (d), respectively.

shift^{72,73} of a quasiparticle. Since the impurity scattering in magnetic fields itself is a difficult problem to solve analytically, we neglect the interplay between magnetic fields and impurity scatterings. Within the phenomenological theory,⁷³ effects of magnetic fields is considered by replacing E in Eq. (46) by $E + |\Delta_0 \cos \gamma \sin \gamma| \phi_B$ as

$$g_B^{(0)} = \int_{-\pi/2}^{\pi/2} d\gamma \frac{\Delta_0^2 \cos^7 \gamma \sin^2 \gamma}{E_B^2 z_0^4 + \Delta_0^2 \cos^6 \gamma \sin^2 \gamma}, \quad (56)$$

$$E_B = E + 2\Delta_0 |\cos \gamma \sin \gamma| \phi_B, \quad (57)$$

$$\phi_B = 2\pi \frac{B \xi_0^2}{\phi_0} \tan \gamma = B_0 \tan \gamma, \quad (58)$$

where $\phi_0 = 2\pi \hbar c/e$ and $B_0 = 1.0^{-3}$ corresponds to $B = 1$ Tesla. A quasiparticle acquires the Aharonov-Bohm like phase shift ϕ_B while moving near the NS interface.⁷³ In a previous paper, we found that ZBCP in clean junctions remains a single peak even in the strong magnetic fields⁷³ as shown in Fig. 7 (c), where $z_0 = 10$ and $T = 0.05 E_{ZEP}$. In Fig. 7 (a) and (b), we show the conductance in the presence of low density strong impurities and high density weak impurities, respectively, where V_i and ρ_i are same as those in Fig. 6 (a) and (b), respectively. A temperature is fixed at $T = 0.05 E_{ZEP}$. In contrast to clean junctions in Fig. 7 (c), the ZBCP in disordered junctions splits into two peaks under magnetic fields as shown in Fig. 7(a). The results within the phenomenological theory indicate that the sensitivity of the ZBCP to magnetic fields depends on the degree of impurity scatterings. In

insets, peak positions (δeV) are plotted with circles as a function of magnetic fields. For high density weak impurities in Fig. 7 (b), we also found that the degree of peak splitting increases with increasing magnetic fields. In the limit of the strong fields, δeV tends to saturate as shown in the inset. These characteristic behavior are found in the experiment.³⁵ Although we have well explained the

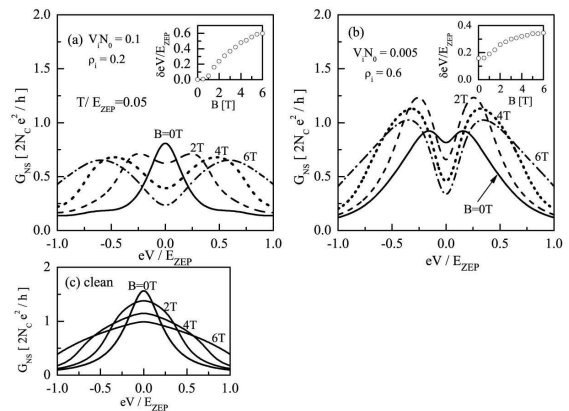


FIG. 7: The conductance under external magnetic fields for low density strong impurities with $V_i N_0 = 0.1$ and $\rho_i = 0.2$ are shown in (a), where T is fixed at $0.05 E_{ZEP}$. Those for high density weak impurities with $V_i N_0 = 0.005$ and $\rho_i = 0.6$ are shown in (b). In insets, peak positions are plotted as a function of magnetic fields. The conductance of clean junctions is shown in (c).

characteristic behavior of the experimental conductance peaks under magnetic fields, the applicability of the phenomenological theory in the presence of impurities is still unclear. This issue would be addressed more clearly in an exact numerical simulation.

IV. DISCUSSION

In experiments, the split of the ZBCP has been reported in overdoped high- T_c superconductors.³⁸ The heavy carrier doping may bring a number of defects or imperfections in superconductors. It is evident that the impurity scattering is unavoidable even in underdoped high- T_c superconductors. The split of the ZBCP would be found in underdoped superconductors if they have bad sample quality. In the same way, the split of the ZBCP would not be found even in overdoped superconductors if their sample quality are good enough. The sample quality is a key factor for the split of the ZBCP. This argument is consistent with an experiment,⁷⁴ where the potential disorder is artificially introduced to the NS junctions by the ion-irradiation and washes out the ZBCP in the limit of strong disorder.

In order to compare the theoretical results in this paper with experiments, we may consider the impurity scattering in normal metals. The total resistance (R) in the dirty normal-metal / (110) d -wave junction can be described simply by $R = R_D + R_{NS}$,^{75,76} where $R_D = 1/G_D$ is the resistance of the dirty normal metal and $G_{NS} = 1/R_{NS}$ is the conductance discussed in this paper. The equation indicates the absence of the proximity effect in the dirty normal metal.^{77,78} The height of the ZBCP can be reduced to reasonable values in the presence of the impurity scattering in normal metals because the total conductance is given by $1/(R_D + R_{NS})$. The degree of splitting depends on parameters such as the potential of impurities (V_j), the position of impurities (x_j) and the transparency of the junction ($T_B \sim 1/z_0^2$). In particular, T_B is the most important parameter. As shown in Figs. 3 and 6, the degree of splitting is roughly given by $E_{ZEP} = \Delta_0/z_0^2 \sim \Delta_0 T_B$. Thus it is possible to choose T_B to fit the degree of splitting with that found in experiments. The amplitude of the pair potential is about 30-40 meV in typical high- T_c materials. The degree of splitting is then estimated to be 1.2-1.6 meV for $z_0 = 5$, which is almost consistent with that found in experiments, for instance, 2 meV.³⁵ It is also necessary to consider electronic structures of high- T_c materials for the quantitative agreement of the splitting width in theories with that in experiments.

In quasiclassical Green function theories, the conductance is proportional to the density of states at the surface of superconductors. We find that E dependence of the density of states at the interface in Eq. (33) is apparently different from that of the conductance even in the clean junctions shown in Eq. (46). We also find that $N_s(E, x = 0) \sim N_0 \ll N_s(E, x = \xi_0)$ as shown in Fig. 2 (b). The density of states near the interface averaged over ξ_0 in this paper may correspond to the surface density of states in the quasiclassical approximation, where the rapidly oscillating part of the wave function are neglected and the smallest length scale is given by ξ_0 . It is impossible to directly compare the present theory with the quasiclassical Green function theories because the position of impurities is a key parameter for the split of the ZBCP in our theory.

The Abrikosov-Gor'kov (AG) theory⁷⁹ is a useful approach to discuss the impurity scattering in superconductors. The applicability of the AG theory is limited to the superconductivity in diffusive metals, where the mean free path is much smaller than the size of the disordered region in superconductors. Here we briefly discuss a relation between the AG theory and ours. Since the AG theory assumes the diffusive transport regime, we define the mean free path of a quasiparticle in the Born approximation,

$$\ell = v_F \tau, \quad (59)$$

$$\frac{\hbar}{\tau} = 2\pi \bar{\rho}_i N_0 V_i^2, \quad (60)$$

$$\bar{\rho}_i = N_i / W L_s, \quad (61)$$

where we consider $W \times L_s$ disordered region on two-dimensional superconductor as in Fig. 6. The impurity density $\bar{\rho}_i$ can be replaced by the dimensionless impurity density $\rho_i = (2\pi/k_F)^2 \bar{\rho}_i$. The ratio of the mean free path and the coherence length is given by

$$\frac{\ell}{\xi_0} = \frac{\Delta_0}{\mu_F} \frac{\pi}{\rho_i (N_0 V_i)^2} \quad (62)$$

In this paper, ℓ/ξ_0 is larger than unity even in the limit of $\rho_i = 1$ because we assume $\Delta_0/\mu_F = 0.1$ and $N_0 V_i < 0.1$. On the other hand, the dirty limit is defined by a relation $\ell/\xi_0 \ll 1$. When we choose L_s being a few coherence length as shown in Fig. 6, where $L_s \sim 3\xi_0$, we find that ℓ/L_s is still larger than unity. The disordered region is not in the diffusive regime but in the quasi-ballistic regime because the diffusive regime is characterized by a relation $\ell/L_s \ll 1$. Thus it is basically impossible to apply the Abrikosov-Gor'kov theory to the model in this paper. The scattering theory⁶⁸ used in this paper is a suitable analytic method to discuss the conductance of such NS junctions. Although the impurity scattering near the interface is very weak in normal states, it drastically affects the conductance below the critical temperature. Impurities located at the resonant states seriously suppress the degree of the resonance even if their potentials are weak. In the AG theory, the real part of the self-energy is usually neglected. In our theory, this approximation corresponds to an equation $s_2 = 0$. However s_2 plays an important role in the peak splitting. When we omit s_2 , I_2 and I_3 must be also zero, which leads to positive Γ_j and no splitting irrespective of $V_i N_0$ and $x_j k_F$.

We show that the impurity scattering causes the splitting of the ZBCP. The conclusion, however, does not deny a possibility of the BTRSS. In a previous paper,³³ we assume the $s + id$ symmetry near the NS interface and numerically study the tunneling conductance. The results show that the split of the ZBCP is insensitive to the potential disorder. Thus peak splitting would be always expected in low transparent junctions³¹ if the BTRSS appears at the NS interface. At present, we have only limited information on the BTRSS within the mean-field theories. To understand the nature of the BTRSS further beyond the mean-field theory, we have to analyze electronic structure of high- T_c superconductors based on microscopic models and make clear effects of the surface, the electron correlation and the random potentials on the superconducting state. This is an important future problem.

Since the formation of the ZES is a universal phenomenon in superconductors with unconventional pairing symmetries, the ZES is also expected at a surface of spin-triplet superconductors.⁸⁰ It is interesting to study effects of impurities on transport properties in spin-triplet superconductor junctions.^{46,78,81,82,83,84,85,86,87,88,89,90,91,92,93,94}

V. CONCLUSION

We have discussed effects of impurity scatterings on the conductance in normal-metal/ d wave superconductor junctions. The conductance is calculated from the Andreev and the normal reflection coefficients which are estimated by using the single-site approximation. We consider impurities near the junction interface on the superconductor side. The strength of the impurity scattering strongly depends on the transparency of the junction, the position of impurities and the energy of a quasiparticle because the ZES are formed at the NS interface. We conclude that the impurity scattering causes the split of the zero-bias conductance peak. The results are consistent with previous numerical simulations. We have also shown that characteristic behaviors of the conductance spectra at finite temperatures and under external magnetic fields qualitatively agree with those reported in experiments.

APPENDIX A: TRANSMISSION AND REFLECTION COEFFICIENTS

In the clean NS junctions, the transmission and the reflection coefficients can be calculated from the appropriate boundary condition of the wave function. The calculated results are shown below.

$$r_{NN}^{he}(l) = \frac{\bar{k}_l^2}{\Xi_l} \frac{\Delta_l}{2} e^{-i\varphi}, \quad (\text{A1})$$

$$r_{NN}^{ee}(l) = \frac{-iz_0(\bar{k}_l - iz_0)}{\Xi_l} E, \quad (\text{A2})$$

$$t_{SN}^{ee}(l) = \frac{\bar{k}_l(\bar{k}_l - iz_0)}{\Xi_l} E u_l e^{-i\varphi/2}, \quad (\text{A3})$$

$$t_{SN}^{he}(l) = \frac{iz_0\bar{k}_l}{\Xi_l} E v_l e^{-i\varphi/2}, \quad (\text{A4})$$

$$r_{NN}^{eh}(l) = \frac{-\bar{k}_l^2}{\Xi_l} \frac{\Delta_l}{2} e^{i\varphi}, \quad (\text{A5})$$

$$r_{NN}^{hh}(l) = \frac{iz_0(\bar{k}_l + iz_0)}{\Xi_l} E, \quad (\text{A6})$$

$$t_{SN}^{hh}(l) = \frac{\bar{k}_l(\bar{k}_l + iz_0)}{\Xi_l} E u_l e^{i\varphi/2}, \quad (\text{A7})$$

$$t_{SN}^{eh}(l) = \frac{iz_0\bar{k}_l}{\Xi_l} E v_l e^{i\varphi/2}, \quad (\text{A8})$$

$$r_{SS}^{he}(l) = \frac{\bar{k}_l^2 + 2z_0^2}{\Xi_l} \frac{\Delta_l}{2}, \quad (\text{A9})$$

$$r_{SS}^{ee}(l) = \frac{-iz_0(\bar{k}_l - iz_0)}{\Xi_l} \Omega_l, \quad (\text{A10})$$

$$t_{NS}^{ee}(l) = \frac{\bar{k}_l(\bar{k}_l - iz_0)}{\Xi_l} \Omega_l u_l e^{i\varphi/2}, \quad (\text{A11})$$

$$t_{NS}^{he}(l) = \frac{-iz_0\bar{k}_l}{\Xi_l} \Omega_l v_l e^{-i\varphi/2}, \quad (\text{A12})$$

$$(\text{A13})$$

$$r_{SS}^{eh}(l) = \frac{-(\bar{k}_l^2 + 2z_0^2)}{\Xi_l} \frac{\Delta_l}{2}, \quad (\text{A14})$$

$$r_{SS}^{hh}(l) = \frac{iz_0(\bar{k}_l + iz_0)}{\Xi_l} \Omega_l, \quad (\text{A15})$$

$$t_{NS}^{hh}(l) = \frac{\bar{k}_l(\bar{k}_l + iz_0)}{\Xi_l} \Omega_l u_l e^{-i\varphi/2}, \quad (\text{A16})$$

$$t_{NS}^{eh}(l) = \frac{-iz_0\bar{k}_l}{\Xi_l} \Omega_l v_l e^{i\varphi/2}, \quad (\text{A17})$$

$$\Xi_l = Ez_0^2 + \bar{k}_l^2 \left(\frac{E + \Omega_l}{2} \right). \quad (\text{A18})$$

For instance, $t_{NS}^{he}(l)$ is the transmission coefficients from the electron branch in a superconductor to the hole branch in a normal metal. In above coefficients, we use a relation $q_l^\pm = k_l^\pm \simeq k_l$ for simplicity. The conclusions in this paper remain unchanged in this approximation.

APPENDIX B: GREEN FUNCTIONS

The real space retarded Green function in clean junctions can be calculated by using the transmission and the reflection coefficients in Appendix A. For $x < x' < 0$, the Green function from a normal metal to a normal metal is

$$\begin{aligned} \hat{G}_0^{NN}(\mathbf{r}, \mathbf{r}') &= -i \frac{\pi N_0}{W} \sum_{k_y^{(l)}} e^{ik_y^{(l)}(y-y')} \\ &\times \left[\frac{1}{q^+} \left\{ \begin{pmatrix} 1 & 0 \\ 0 & 0 \end{pmatrix} e^{iq_l^+ |x-x'|} + \begin{pmatrix} 0 & 0 \\ 1 & 0 \end{pmatrix} e^{iq_l^- x} e^{-iq_l^+ x'} r_{NN}^{he}(l) + \begin{pmatrix} 1 & 0 \\ 0 & 0 \end{pmatrix} e^{-iq_l^+(x+x')} r_{NN}^{ee}(l) \right\} \right. \\ &\quad \left. + \frac{1}{q^-} \left\{ \begin{pmatrix} 0 & 0 \\ 0 & 1 \end{pmatrix} e^{-iq_l^- |x-x'|} + \begin{pmatrix} 0 & 1 \\ 0 & 0 \end{pmatrix} e^{-iq_l^+ x} e^{iq_l^- x'} r_{NN}^{eh}(l) + \begin{pmatrix} 0 & 0 \\ 0 & 1 \end{pmatrix} e^{iq_l^-(x+x')} r_{NN}^{hh}(l) \right\} \right], \quad (\text{B1}) \\ N_0 &= \frac{m}{\pi \hbar^2}. \quad (\text{B2}) \end{aligned}$$

For $x > x' > 0$, the Green function from a superconductor to a superconductor is

$$\begin{aligned} \hat{G}_0^{SS}(\mathbf{r}, \mathbf{r}') &= -i \frac{\pi N_0}{W} \sum_{k_y^{(l)}} e^{ik_y^{(l)}(y-y')} \frac{E}{\Omega_l} \\ &\times \hat{\Phi} \left[\frac{1}{k^+} \left\{ \begin{pmatrix} u_l^2 & u_l v_l \\ u_l v_l & v_l^2 \end{pmatrix} e^{ik_l^+ |x-x'|} + \begin{pmatrix} -u_l v_l & v_l^2 \\ u_l^2 & -u_l v_l \end{pmatrix} e^{-ik_l^- x + ik_l^+ x'} r_{SS}^{he}(l) + \begin{pmatrix} u_l^2 & -u_l v_l \\ u_l v_l & -v_l^2 \end{pmatrix} e^{ik_l^+(x+x')} r_{SS}^{ee}(l) \right\} \right. \\ &\quad \left. + \frac{1}{k^-} \left\{ \begin{pmatrix} v_l^2 & -u_l v_l \\ -u_l v_l & u_l^2 \end{pmatrix} e^{-ik_l^- |x-x'|} + \begin{pmatrix} u_l v_l & u_l^2 \\ v_l^2 & u_l v_l \end{pmatrix} e^{ik_l^+ x - ik_l^- x'} r_{SS}^{eh}(l) + \begin{pmatrix} -v_l^2 & -u_l v_l \\ u_l v_l & u_l^2 \end{pmatrix} e^{-ik_l^-(x+x')} r_{SS}^{hh}(l) \right\} \right] \hat{\Phi}^*, \quad (\text{B3}) \\ \hat{\Phi} &= \begin{pmatrix} e^{i\frac{\varphi}{2}} & 0 \\ 0 & e^{-i\frac{\varphi}{2}} \end{pmatrix}, \quad (\text{B4}) \end{aligned}$$

where φ is the phase of a superconductor. For $x > 0 > x'$, the Green function from a normal metal to a superconductor is

$$\begin{aligned} \hat{G}_0^{SN}(\mathbf{r}, \mathbf{r}') &= -i \frac{\pi N_0}{W} \sum_{k_y^{(l)}} e^{ik_y^{(l)}(y-y')} \\ &\times \hat{\Phi} \left[\frac{1}{q^+} \left\{ \begin{pmatrix} u_l & 0 \\ v_l & 0 \end{pmatrix} e^{ik_l^+ x - iq_l^+ x'} t_{SN}^{ee}(l) + \begin{pmatrix} -v_l & 0 \\ u_l & 0 \end{pmatrix} e^{-ik_l^- x - iq_l^+ x'} t_{SN}^{he}(l) \right\} \right. \\ &\quad \left. + \frac{1}{q^-} \left\{ \begin{pmatrix} 0 & -v_l \\ 0 & u_l \end{pmatrix} e^{-ik_l^- x + iq_l^- x'} t_{SN}^{hh}(l) + \begin{pmatrix} 0 & u_l \\ 0 & v_l \end{pmatrix} e^{ik_l^+ x + iq_l^- x'} t_{SN}^{eh}(l) \right\} \right]. \quad (\text{B5}) \end{aligned}$$

For $x < 0 < x'$, the Green function from a superconductor to a normal metal is

$$\begin{aligned} \hat{G}_0^{NS}(\mathbf{r}, \mathbf{r}') &= -i \frac{\pi N_0}{W} \sum_{k_y^{(l)}} e^{ik_y^{(l)}(y-y')} \frac{E}{\Omega_l} \\ &\times \left[\frac{1}{k^+} \left\{ \begin{pmatrix} u_l & -v_l \\ 0 & 0 \end{pmatrix} e^{-iq_l^+ x + ik_l^+ x'} t_{NS}^{ee}(l) + \begin{pmatrix} 0 & 0 \\ u_l & -v_l \end{pmatrix} e^{iq_l^- x + ik_l^+ x'} t_{NS}^{he}(l) \right\} \right. \\ &\quad \left. + \frac{1}{k^-} \left\{ \begin{pmatrix} 0 & 0 \\ v_l & u_l \end{pmatrix} e^{iq_l^- x - ik_l^- x'} t_{NS}^{hh}(l) + \begin{pmatrix} v_l & u_l \\ 0 & 0 \end{pmatrix} e^{-iq_l^+ x - ik_l^- x'} t_{NS}^{eh}(l) \right\} \right] \hat{\Phi}^*. \quad (\text{B6}) \end{aligned}$$

* Electronic address: asano@eng.hokudai.ac.jp

¹ C. R. Hu, Phys. Rev. Lett. **72**, 1526 (1994).

² S. Kashiwaya and Y. Tanaka, Rep. Prog. Phys. **63**, 1641 (2001).

- ³ Y. Tanaka and S. Kashiwaya, Phys. Rev. Lett. **74**, 3451 (1995).
- ⁴ S. Kashiwaya, Y. Tanaka, M. Koyanagi, H. Takashima, and K. Kajimura, Phys. Rev. B **51**, 1350 (1995).
- ⁵ L. Alff, H. Takashima, S. Kashiwaya, N. Terada, H. Ihara, Y. Tanaka, M. Koyanagi, and K. Kajimura, Phys. Rev. B **55**, 14757 (1997).
- ⁶ W. Wang, M. Yamazaki, K. Lee, and I. Iguchi, Phys. Rev. B **60**, 4272 (1999).
- ⁷ J. Y. T. Wei, N. -C. Yeh, D. F. Garrigus, and M. Strasik, Phys. Rev. Lett. **81**, 2542 (1998).
- ⁸ I. Iguchi, W. Wang, M. Yamazaki, Y. Tanaka, and S. Kashiwaya, Phys. Rev. B **62**, R6131 (2000).
- ⁹ J. Geerk, X. X. Xi, and G. Linker, Z. Phys. B. **73**, 329 (1988).
- ¹⁰ Z. Q. Mao, M. M. Rosario, K. D. Nelson, K. Wu, I. G. Deac, P. Schiffer, Y. Liu, T. He, K. A. Regan, and R. J. Cava, Phys. Rev. B **67**, 094502 (2003).
- ¹¹ Y. S. Barash, H. Burkhardt, and D. Rainer, Phys. Rev. Lett. **77**, 4070 (1996).
- ¹² Y. Tanaka and S. Kashiwaya, Phys. Rev. B **53**, R11957 (1996).
- ¹³ Y. Tanaka and S. Kashiwaya, Phys. Rev. B **56**, 892 (1997).
- ¹⁴ Y. Tanaka and S. Kashiwaya, Phys. Rev. B **58**, R2948 (1998).
- ¹⁵ Y. Tanaka and S. Kashiwaya, J. Phys. Soc. Jpn. **68**, 3485 (1999); J. Phys. Soc. Jpn. **69**, 1152 (2000).
- ¹⁶ Y. Asano, Phys. Rev. B **64**, 224515 (2001).
- ¹⁷ H. Arie, Y. Yasuda, H. Kobayashi, I. Iguchi, Y. Tanaka, and S. Kashiwaya, Phys. Rev. B **62**, 11864 (2000).
- ¹⁸ E. Il'chev, V. Zakosarenko, R. P. IJsselsteijn, V. Schultze, H. -G. Mayer, H. E. Hoenig, H. Hilgenkamp, and J. Mannhart, Phys. Lev. Lett. **81**, 894 (1998).
- ¹⁹ E. Il'chev, M. Grajcar, R. Hlubina, R. P. IJsselsteijn, H. E. Hoenig, H. -G. Mayer, A. Golubov, M. H. S. Amin, A. M. Zagoskin, A. N. Omelyanchouk, and M. Yu. Kupriyanov, Phys. Lev. Lett. **86**, 5369 (2001).
- ²⁰ S. Shirai, H. Tsuchiura, Y. Asano, Y. Tanaka, J. Inoue, Y. Tanuma, and S. Kashiwaya, J. Phys. Soc. Jpn. **72**, 2299 (2003).
- ²¹ G. Testa, A. Monaco, E. Esosito, E. Sarelli, D. -J. Kang, E. J. Tarte, S. H. Mennema, and M. G. Blamire, cond-mat/0310727.
- ²² A. F. Andreev, Zh. Eksp. Theor. Fiz, **46**, 1823 (1964) [Sov. Phys. JETP **19**, 1228 (1964)].
- ²³ M. Fogelström, D. Rainer, and J. A. Sauls, Phys. Rev. Lett. **79**, 281 (1997); D. Rainer, H. Burkhardt, M. Fogelström, and J. A. Sauls, J. Phys. Chem. Solids **59**, 2040 (1998).
- ²⁴ Y. Tanaka, H. Tsuchiura, Y. Tanuma, and S. Kashiwaya, J. Phys. Soc. Jpn. **71**, 271 (2002).
- ²⁵ Y. Tanaka, H. Itoh, H. Tsuchiura, Y. Tanuma, J. Inoue, and S. Kashiwaya, J. Phys. Soc. Jpn. **71**, 2005 (2002).
- ²⁶ Y. Tanaka, Y. Tanuma, K. Kuroki, and S. Kashiwaya J. Phys. Soc. Jpn. **71**, 2102 (2002).
- ²⁷ S. Kashiwaya, Y. Tanaka, M. Koyanagi, and K. Kijimura, J. Phys. Chem. Solids **56**, 1721 (1995).
- ²⁸ M. Matsumoto and H. Shiba, J. Phys. Soc. Jpn. **64**, 4867 (1995).
- ²⁹ Y. Tanuma, Y. Tanaka, M. Ogata, and S. Kashiwaya, J. Phys. Soc. Jpn. **67**, 1118 (1998).
- ³⁰ Y. Tanuma, Y. Tanaka, M. Ogata, and S. Kashiwaya, Phys. Rev. B **60**, 9817 (1999).
- ³¹ Y. Tanuma, Y. Tanaka, and S. Kashiwaya, Phys. Rev. B **64**, 214519 (2001).
- ³² I. Lubimova and G. Koren, cond-mat/0306030.
- ³³ N. Kitaura, H. Itoh, Y. Asano, Y. Tanaka, J. Inoue, Y. Tanuma, and S. Kashiwaya, J. Phys. Soc. Jpn. **72**, 1718 (2003).
- ³⁴ R. B. Laughlin, Phys. Rev. Lett. **80**, 5188 (1998).
- ³⁵ M. Covington, M. Aprili, E. Paraoanu, L. H. Greene, F. Xu, J. Zhu, and C. A. Mirkin, Phys. Rev. Lett. **79**, 277 (1997).
- ³⁶ A. Biswas, P. Fournier, M. M. Qazilbash, V. N. Smolyaninova, H. Balci, and R. L. Greene, Phys. Rev. Lett. **88**, 207004 (2002).
- ³⁷ Y. Dagan and G. Deutscher, Phys. Rev. Lett. **87**, 177004 (2001).
- ³⁸ A. Sharoni, O. Millo, A. Kohen, Y. Dagan, R. Beck, G. Deutscher, and G. Koren, Phys. Rev. B **65**, 134526 (2002).
- ³⁹ A. Kohen, G. Leibovitch, and G. Deutscher, Phys. Rev. Lett. **90**, 207005 (2003).
- ⁴⁰ L. H. Greene, P. Hentges, H. Aubin, M. Aprili, E. Badica, M. Covington, M. M. Pafford, G. Westwood, W. G. Klemperer, S. Jian, D. G. Hinks, Physica C **387**, 162 (2003).
- ⁴¹ M. Aprili, E. Badica, and L. H. Greene, Phys. Rev. Lett. **83**, 4630 (1999).
- ⁴² R. Krupke and G. Deutscher, Phys. Rev. Lett. **83**, 4634 (1999).
- ⁴³ J. W. Ekin, Y. Xu, S. Mao, T. Venkatesan, D. W. Face, M. Eddy, and S. A. Wolf, Phys. Rev. B **56**, 13746 (1997).
- ⁴⁴ A. Sawa, S. Kashiwaya, H. Obara, H. Yamasaki, M. Koyanagi, Y. Tanaka, and N. Yoshida, Physica C **339**, 107 (2000).
- ⁴⁵ H. Aubin, L. H. Greene, S. Jian, and D. G. Hinks, Phys. Rev. Lett. **89**, 177001 (2002).
- ⁴⁶ T. Hirai, Y. Tanaka, N. Yoshida, Y. Asano, J. Inoue, and S. Kashiwaya, Phys. Rev. B **67**, 174501 (2003).
- ⁴⁷ N. Yoshida, Y. Asano, H. Itoh, Y. Tanaka, and J. Inoue, J. Phys. Soc. Jpn. **72**, 895 (2003).
- ⁴⁸ Y. Asano and Y. Tanaka, Phys. Rev. B **65**, 064522 (2002).
- ⁴⁹ Y. Asano, Phys. Rev. B **63**, 052512 (2001).
- ⁵⁰ Y. Asano and Y. Tanaka, "Toward the controllable Quantum State" Eds. H. Takayanagi and J. Nitta, pp 185 (World Scientific, Singapore, 2003).
- ⁵¹ Y. S. Barash, A. A. Svidzinsky, and H. Burkhardt, Phys. Rev. B **55**, 15282 (1997).
- ⁵² A. A. Golubov and M. Y. Kupriyanov, Pis'ma Zh. Eksp. Teor. fiz **69**, 242 (1999).[Sov. Phys. JETP Lett. **69**, 262 (1999).]; **67**, 478 (1998).[Sov. Phys. JETP Lett. **67**, 501 (1998).]
- ⁵³ A. Poenicke, Yu. S. Barash, C. Bruder, and V. Istyukov, Phys. Rev. B **59**, 7102 (1999).
- ⁵⁴ K. Yamada, Y. Nagato, S. Higashitani, and K. Nagai, J. Phys. Soc. Jpn. **65**, 1540 (1996).
- ⁵⁵ Y. Tanaka, Y. Tanuma, and S. Kashiwaya, Phys. Rev. B **64**, 054510 (2001).
- ⁵⁶ T. Lück, U. Eckern, and A. Shelankov, Phys. Rev. B **63**, 064510 (2001).
- ⁵⁷ G. Eilenberger, Z. Phys. **214**, 195 (1968).
- ⁵⁸ A. I. Larkin and Yu. N. Ovchinnikov, Eksp. Teor. Fiz. **55**, 2262 (1986).[Sov. Phys. JETP **28**, 1200 (1968).]
- ⁵⁹ A. V. Zaitsev, Zh. Eksp. Teor. Fiz. **86**, 1742 (1984). [Sov. Phys. JETP **59**, 1015 (1984).]
- ⁶⁰ A. L. Shelankov, J. Low. Tem. Phys. **60**, 29 (1985).
- ⁶¹ C. Bruder, Phys. Rev. B **41**, 4017 (1990).
- ⁶² P. A. Lee and D. S. Fisher, Phys. Rev. Lett. **47**, 882 (1981).

- ⁶³ G. E. Blonder, M. Tinkham, and T. M. Klapwijk, Phys. Rev. B **25**, 4515 (1982).
- ⁶⁴ Y. Takane and H. Ebisawa, J. Phys. Soc. Jpn. **61**, 1685 (1992).
- ⁶⁵ P. G. de Gennes, *Superconductivity of Metals and Alloys*, (Benjamin, New York, 1966).
- ⁶⁶ Y. Tanaka, T. Asai, N. Yoshida, J. Inoue, and S. Kashiwaya, Phys. Rev. B **61**, R11902 (2000).
- ⁶⁷ S. Nonoyama, A. Nakamura, Y. Aoyagi, T. Sugano, and A. Okiji, Phys. Rev. B **47**, 2423 (1993).
- ⁶⁸ Y. Asano and G. E. W. Bauer, Phys. Rev. B **54**, 11602 (1996); Erratum **54**, 9972 (1997).
- ⁶⁹ Y. Tanuma, Y. Tanaka, M. Yamashiro, and S. Kashiwaya, Phys. Rev. B **57**, 7997 (1998).
- ⁷⁰ Y. Tanaka and S. Kashiwaya, Phys. Rev. B **53**, 9371 (1996).
- ⁷¹ M. Matsumoto and H. Shiba, J. Phys. Soc. Jpn. **64**, 1703 (1995).
- ⁷² Y. Asano, Phys. Rev. B **61**, 1732 (2000); Y. Asano and T. Kato, J. Phys. Soc. Jpn. **69**, 1125 (2000); Y. Asano and T. Yuito, Phys. Rev. B **62**, 7477 (2000).
- ⁷³ Y. Asano, Y. Tanaka, and S. Kashiwaya, cond-mat/0302287.
- ⁷⁴ M. Aprili, M. Covington, E. Paraoanu, B. Niedermeier, and L. H. Greene, Phys. Rev. B **57**, R8139 (1998).
- ⁷⁵ Y. Tanaka, Yu. Nazarov, and S. Kashiwaya, Phys. Rev. Lett. **90**, 167003 (2003).
- ⁷⁶ H. Kashiwaya, I. Kurosawa, S. Kashiwaya, A. Sawa, and Y. Tanaka, Phys. Rev. B **68**, 054527 (2003).
- ⁷⁷ Y. Asano, Phys. Rev. B **64**, 014511 (2001).
- ⁷⁸ Y. Asano, J. Phys. Soc. Jpn. **71**, 905 (2002).
- ⁷⁹ A. A. Abrikosov, L. P. Gor'kov, and I. E. Dzyaloshinskii, *Quantum Field Theoretical Methods in Statistical Physics*, (Pergamon Press, London, 1963).
- ⁸⁰ L. J. Buchholtz and G. Zwicknagl, Phys. Rev. B **23**, 5788 (1981).
- ⁸¹ M. Yamashiro, Y. Tanaka, and S. Kashiwaya, Phys. Rev. B **56**, 7847 (1997).
- ⁸² M. Yamashiro, Y. Tanaka, Y. Tanuma, and S. Kashiwaya, J. Phys. Soc. Jpn. **67**, 3224 (1998).
- ⁸³ M. Yamashiro, Y. Tanaka, N. Yoshida, and S. Kashiwaya, J. Phys. Soc. Jpn. **68**, 2019 (1999).
- ⁸⁴ Y. Asano, Y. Tanaka, Y. Matsuda, and S. Kashiwaya, Phys. Rev. B **68**, 184506 (2003).
- ⁸⁵ N. Yoshida, Y. Tanaka, J. Inoue, and S. Kashiwaya, J. Phys. Soc. Jpn. **68**, 1071 (1999).
- ⁸⁶ T. Hirai, N. Yoshida, Y. Tanaka, J. Inoue, and S. Kashiwaya, J. Phys. Soc. Jpn. **70**, 1885 (2001).
- ⁸⁷ Y. Tanuma, K. Kuroki, Y. Tanaka, and S. Kashiwaya, Phys. Rev. B **64**, 214510 (2001).
- ⁸⁸ Y. Tanuma, K. Kuroki, Y. Tanaka, R. Arita, S. Kashiwaya, and H. Aoki, Phys. Rev. B **65**, 064522 (2002).
- ⁸⁹ Y. Tanaka, T. Hirai, K. Kusakabe, and S. Kashiwaya, Phys. Rev. B **60**, 6308 (1999).
- ⁹⁰ C. Honerkamp and M. Sigrist, J. Low. Temp. Phys. **111**, 898 (1998); Prog. Theor. Phys. **100**, 53 (1998).
- ⁹¹ N. Stefanakis, Phys. Rev. B **64**, 224502 (2001); J. Phys. Cond. Matt. **13**, 3643 (2001).
- ⁹² K. Sengupta, I. Žutić, H.-J. Kwon, V. M. Yakovenko, and S. Das Sarma, Phys. Rev. B **63**, 144531 (2001).
- ⁹³ Y. Asano and K. Katabuchi, J. Phys. Soc. Jpn. **71**, 1974 (2002).
- ⁹⁴ Y. Asano, Y. Tanaka, M. Sigrist, and S. Kashiwaya, Phys. Rev. B **67**, 184505 (2003).